Object Identification from Hazed Images, Improving the Boundaries and Corners using KOA Techniques

Buvanesh Pandian V[1], Arun Prasath T[2], Pallikonda Rajasekaran M[3], Kottaimalai R[4].

[1]Department of EEE, Kalasalingam Academy of Research and Education, India.
[2]Department of Biomedical, Kalasalingam Academy of Research and Education, India.
[3]Department of ECE, Kalasalingam Academy of Research and Education, India.
[4]Department of ECE, Kalasalingam Academy of Research and Education, India.

ARTICLE INFO	ABSTRACT
	Mist, smoke, and fog will cause objects or images taken from far-off places to be of poor quality and invisible. Here, we use the Optimal Adaptive method (KOA) and K-Means Clustering to rub out or eliminate the undesirable hazes from the image. The photos are first grouped by color clustering using K-Means Clustering (KMC). Our approach greatly benefits from an analysis of the transmission function's intrinsic boundary limitation. To forecast the transmission of the unknown scene, this constraint is treated as an optimization problem. Furthermore, variable splitting methodology-based transmission refinement strategies are employed to address the problem. The suggested approach may recover haze-free, high-quality photos with original colors and improved image information with just a few general assumptions, such as the "K" value and "ω." The results of the experiment, which used evaluation settings and produced 88.07% for our suggested method, show the efficiency and efficacy of the suggested technique with a large number of hazy photos. The suggested work produces better results in FSIM and SSIM when compared to the results that are already available.

Keywords: Image Dehazing, Global air light, transmission refining, Boundary constraints, K-Means Clustering.

1. Introduction

Dehazing has received plenty of interest in the image processing field for the past few years as a difficult and poorly presented subject. Better quality image sharing extensive information is critical to current computer vision applications such as image classification, aerial imaging, semantic segmentation, and object identification. Poor lighting and environmental conditions, including fog, mist, pollution, and human factors, greatly reduce camera image visibility and quality, which makes it difficult to apply computer vision algorithms. Because of this, image dehazing techniques have advanced quickly in recent years, making it possible to remove low-quality photos and effectively aid in the restoration of hazy photographs. Image quality is lowered by the presence of suspended particles in the air and the influence of ambient light. When ambient lights are reflected in the eyes by suspended particles, which may contain dust, droplets of water, and other impurities it results in images of small white that make it difficult to distinguish between structures and objects. For restoration and enhancement, many color images are tested for fog reduction factor [1], and image scrambling and pixel replacement are done for the removal of fog [2]. The low-frequency and high-frequency sub-images are subjected to wavelet de-noising and non-local dehazing, respectively, to further minimize haze and noise. At last the reconstruction of sub-images yields a haze-free image [3] and in-depth information about the hazed image [4].

Edge Tracked Scale Normalization (ETSN) is used as normalization with edge detection to remove undesirable background features using Discrete Wavelet Transform [5] and for the segmentation process, the X-ray can also be used [6], [7]. The threshold technique is used for noise removal with a wavelet approach [8]. The K-Means Clustering (KMC) algorithm is used to split the images into smaller parts to provide information. It is also used to increase the brightness level and distortion of image color [9]. Based on the segmentation results, the weights are assigned to the image when the scattering is present in the image from restoration [10]. The priority of

the red color in the RGB space uses this KMC as a morphological process for contrast improvement in images [11]. The KMC and ASFC are used in the reconstruction of an image when the images are in the low-frequency region [12]. For recovering the image scene, the non-local prior methods are used for contrast improvement using patch-based image techniques [13]. When dividing the images into n-parts, the harmful interference in the correlated images can be improved and the brightness of the images also can be increased using the recovery formula [14]. For multi-exposure images, gamma correction and Laplacian pyramid are used [15], [16]. For color attenuation, the Gaussian mixture model is used for the estimation of images [17]. The fuzzy C-means algorithm uses pixel-level estimation in images for non-global values [18]. In order to remove haze from the photos, patches are ranked in order of importance using the dark channel [19]. In order to transmit the image's pixels, the foreground and background are eliminated using the dark channel previous approach [20]. Satellite-based remote sensing data, especially those in the visible light spectrum, are vulnerable to particles that are suspended throughout the imaging process. To overcome this problem, a number of dehazing projects and initiatives have been carried out recently. Their objective is to instantly restore a single jumbled bit of data without any additional information [21]. From the literature survey, it can be concluded that the existing work has some flaws in improving boundaries. Among the issues with the aforementioned algorithms are (i) a high sense of noise and artifacts (iv) a lack of robustness in optimization (v) cluster overlapping; (ii) longer processing times; (iii) reduced accuracy in blurry images. To solve the aforementioned issues, this work employs a unique framework that makes use of KOA algorithms. Consequently, several of the constraints were fixed in this study. They're

- Its goal was to quickly ascertain the viability and correctness of hazed photographs.
- Reducing the amount of cluster overlap.

2.   Proposed Method.

This paper uses a fused model of the K-means algorithm and optimal adaptive techniques are used for the dehazing of a hazed image. Employing an ideal adaptive to repair or reconstruct data through decreasing noise without substantially blurring the image's structural features is routine. The process of the proposed work is expressed in Figure 1.
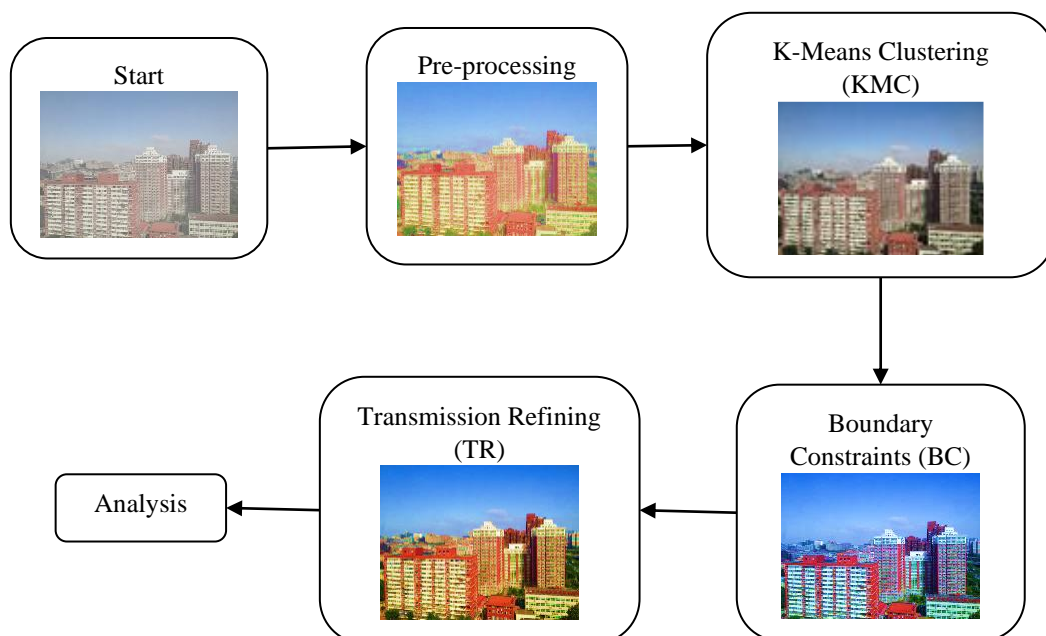

Fig. 1 Proposed work

2.1. Pre Processing

In the pre-processing stage, the global air light method is used. This technique has two steps, namely an estimation of all channels of image and dark channel computing. Haze can be detected channel by the channel at first. An image is estimated by using the RGB (Red-Green-Blue) channel to estimate the image at each channel. After that, the RGB is changed to HSV (Hue-Saturation-Value). The names of the colors in our image are

represented numerically by this HSV scale. To see the global air light at each channel, a dark channel is finally calculated. Stated differently, the air-light component in a haze-free image is estimated using the Global Air-Light technique. It's frequently used to make photos taken in foggy or hazy circumstances more visible. The method works by analyzing the intensity values of each channel (e.g., RGB) and identifying the pixels with the highest intensity values, which are assumed to be the air-light components. The dark channel is calculated by applying the minimum filter across each RGB channel of the image and selecting the minimum value at each pixel. Because non-sky areas in a haze-free outdoor image frequently have some pixels with very low intensity in at least one color channel, this technique is frequently employed in haze removal algorithms to assess the quantity of haze. The dark channel is then separated by subtracting the air-light component from the original image. To compute the dark channel, a minimum filter with window size 'ω' is used. The pre-processing steps should follow two conditions namely, (i) Converting the different image sizes into 16 X 16. Here we are not using any up-sample techniques. Just we are bringing all the unequal sizes to 16 x 16, by using code (ii) Image can be obtained in PNG or jpg format.

$$I_{DCP} = \min_{x \in \omega(k)} \left(\min_{y \in \{R,G,B\}} I(y) \right) \qquad (1)$$

I_{DCP} = Image's dark channel.
$I(y)$ = Initial image.

2.2.   KMC Algorithm.

K-means clustering can be applied to group similar images together based on their size features. From the pre-processing steps, the input of KMC algorithms is noise reduction in images and the desired number of clusters (K). The KMC algorithm gets an input as dark channel values. Dark channel values are pixel intensity values derived from an image's dark channel. The dark channel highlights the darkest pixels in each neighbourhood across the color channels of an image, capturing the regions that are least affected by ambient light. Clustering pixels with similar color or texture characteristics can separate different objects or regions, allowing for further analysis, object recognition, or computer vision tasks. After the pre-processed image is fed into the K-means Clustering (KMC) algorithm, each pixel is indeed allocated to one of the k clusters, which represent differently "means" or centroid colors. The steps are

1. Initial Clustering
2. Pixel Assignment to Clusters
3. Generating the Output Image

If k=3, the final output image might show:

• Region 1 in a light color (e.g., sky)
• Region 2 in a medium color (e.g., mid-tones like vegetation)
• Region 3 in a dark color (e.g., shadowed areas or trees). Table 1 describes the procedure for KMC algorithm work done in MATLAB software. Choosing the value of 'k' in K-means clustering is crucial, as it directly impacts the segmentation quality and usefulness of the final image. The Silhouette Score Analysis, which compares a pixel's similarity to its assigned cluster to other clusters, is what we've employed here. Clusters that are more distinct and well-separated have a higher silhouette score.

Table 1. Procedure for the KMC algorithm

	KMC algorithm procedure
1	Read image
2	Enter the value of K.
3	Making the vectors for the image
4	Initialization of the KMC algorithm
5	Plot the pixel in 3-D
6	Loop for allocating the samples to a mean and then re-updating the means
7	Plot the data with the current means
8	Plot the pixels allocated to the means in different colors
9	Displaying results

Figure 2 picturizes the 3D plot of pixels in RGB space after K-means clustering. Each point represents a pixel, with colors corresponding to the cluster to which it belongs. The red "X" markers indicate the centroids of

each cluster. This visualization shows how pixels with similar RGB values are grouped, revealing the color structure in the image based on clustering.
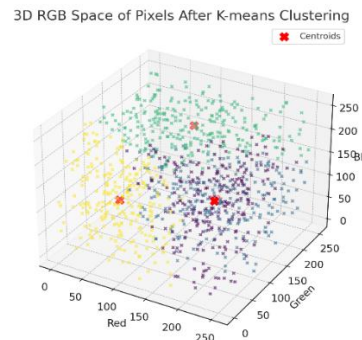

Fig.2. 3D plot of pixels in RGB space.

To visualize pixels allocated to each cluster, the proposed algorithm plots them in different colors according to their assigned mean (cluster centroid). Each cluster will have a distinct color to show the segmentation effect clearly as shown in Figure 3.
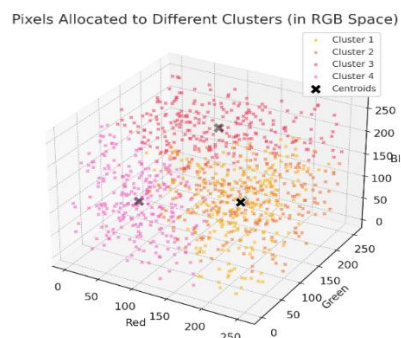

Fig.3. Plotting the pixels allocated to the means in different colors

2.3.   *Optimal Adaptive Technique (OAT).*

Clustering can lead to artifacts at cluster boundaries or over-segmented regions. Adaptive techniques minimize these artifacts by smoothing transitions and ensuring consistent haze removal across the image. A clustered or segmented version of the hazy image is the input given to Optimal Adaptive techniques. It is a technique used for adaptively adjusting the edge detection parameters to accurately detect edges in images with varying levels of noise and contrast. The parameters are optimised in these techniques by using a Differential Filter Bank, Normalizing Filter and Weighting Function. It processes in two stages namely

- Boundary Constraints (BC)
- Transmission Refining (TR)

The overall work process of optimizing the input images after KMC as the segmented version of hazy images is processed in different stages in OAT is explained in Table 2.

Table 2. Stages in OAT by input Optimization

STAGES	WORKS
Input	Clustered image and initial transmission map from k-means clustering.
Boundary Constraints	• Identify cluster boundaries and enforce smooth transitions. • Use weighted averaging or edge-preserving regularization at boundaries.

Transmission Refinement	• Refine the transmission map within each cluster. • Ensure alignment with local image structures using guided filtering. • Regularize to maintain smoothness and preserve edges.
Output	A refined transmission map with smooth transitions across cluster boundaries and accurate haze removal.

2.3.1. BC.

A contour boundary marks a transition in pixel from one image to another in this context. Visual images are evaluated by a computerized system to produce boundaries. Then, we are assuming a window size of 3. The features of morphological work are worked most appropriately. Table 3 explains three different stages and its process in boundary constraints.

Table 3. Process in Boundary Constraints

STAGES	PROCESS
PWT	An input image will be divided into smaller patches for PWT. All patch is processed independently. To construct the final output image, the many processed patches are reassembled. There are various advantages to focusing on certain areas rather than the full images.
PWB	A pixel is commonly thought of as the lowest individual piece. Pixels can be measured in a variety of ways based on their inch and line. The pixel of an image within its limits is discovered independently for R-G-B colors in this case. Here it is used to check all the pixels from the patch-wise transmission.
MF	The minimum filter is the set of pixels that make up a picture's minimum in a specific location. The minimum filter is typically applied to an image to remove positive outlier noise. The structure element decomposition is utilized in this step. An element of structure breakdown approach is used to speed up computations when performing morphological processing of images by splitting an element of structure into fewer simpler parts. This process is done to smoothen the image pixel from the previous stage.

2.3.2. TR.

It is among the most important steps in the dehazing of a single image. The amount of scene light that is hazed and ultimately reaches the image sensor is described by the estimation of each pixel. Each of the used hypotheses must be simultaneously preserved in the perfect solution of the function to compute the transmissions. Each image's size, columns, and rows are considered for this step.

DFB.

A "filter bank," which is an arrangement of band-pass filters, divides the original signal as various signals of images. For a safety measure, the original matrix order keeps the image size maintained which is typically in the odd term.

NF.

This will alter the range of pixel intensity values. Histogram stretching or contrast stretching are other terms for normalization. When applying a filter to an image, it is sometimes helpful to maintain the local illumination level for the output image above that of the input. Each filter coefficient is normalized to add up to one to do this.

WF.
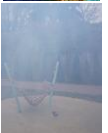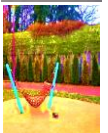
The precise difference between a pixel's intensity and the reference greyscale's brightness level is known as the weight. What a certain pixel symbolizes is determined by its pixel weight, which can be anything from 0 to 1. A pixel having a weight equal to one is an object component. A pixel weighting 0 is considered to be in the background. A pixel weighting 0 to 1 is considered to be located on the outermost boundary of an object.

3.   RESULT AND DISCUSSION

3.1. Qualitative analysis

Here the freely available dataset is obtained from O-haze, and tested in MATLAB software. The obtained results from the proposed works are qualitatively analysed, as shown in Table 4. The 42 different kinds of dehazing images are tested with the SOTS dataset having input ass hazed and output as dehazed.

Table 4. Qualitative analysis

3.2. Quantitative Analysis.

As a result, Quantitative analysis is done with the help of Evaluation Parameters (EP). In this work, the five different EPs are used, namely

  i. Gray scale value.
  ii. FSIM.
  iii. SSIM.
  iv. Contrast.
  v. Time period.
  vi. MSE
  vii. PSNR
  viii. F1 score

3.2.1. Gray scale value.

It is a simplified representation of an image, where each pixel is represented by a single intensity value, ranging from black (0) to white (255).

3.2.2. FSIM.

It is used for measuring the similarity between two images based on their features. FSIM is used to evaluate the quality of compressed, distorted, or modified images. FSIM is calculated using the following formula:

$$FSIM\ (I_1, I_2) = \sum w(i) * f(i)(I_1, I_2) \qquad (2)$$

Where I_1 and I_2 are the input images being compared, $f(i)(I_1, I_2)$ is the local feature similarity at a particular image location, and $w(i)$ is the weight assigned to that local feature similarity. The sum is taken over all image locations. It provides a quantitative measure of image similarity that can be used to evaluate the performance of image processing algorithms or compare the quality of different images. The average value of FSIM ranges from 0.8 to 0.9.

3.2.3. SSIM.

It is used for evaluating the similarity between two images based on its structure. It offers a numerical score that indicates how similar an image is to a reference image. By comparing the structural information and texture details, SSIM can accurately estimate an image's perceived quality. The SSIM index ranges between -1 and 1, where 1 indicates perfect similarity between the two images, 0 indicates no similarity, and -1 indicates perfect dissimilarity or complete mismatch between the images. The best quality for SSIM technique ranges are 0.97, 0.98, and 0.99 and our proposed work is getting an output of 0.9712.

3.2.4. Contrast.

Contrast value is often used as a criterion for segmenting objects from the background in image analysis tasks. It is often used to identify defects, anomalies, or inconsistencies in images. The value of contrast should be expressed in percentage. For humans, the contrast range should be 60% to 70%. Our proposed work is obtaining a result of 65.89.

3.2.5. Time period.

The term "time period" often refers to the duration or period within which an image was shot or reflected. Depending on the context, it can relate to several characteristics of time in images. In general, it is defined as the whole time needed to finish the work from the beginning to the end. The shorter the time period, the faster the result. The time period is always expressed in seconds. In our proposed work, we are obtaining 8.15. The Quantitative Analysis for Evaluation Parameters is displayed in Table 5.

3.2.6. MSE.

Mean Squared Error (MSE) is used for evaluating the quality of image restoration or reconstruction tasks. In general, a lower MSE indicates better performance, as it signifies that the reconstructed image will be closer to the original, ground truth image.

3.2.7. PSNR

It is particularly used to reconstruct or process images. It measures the ratio between the maximum possible power of a signal (the "peak" signal) and the power of corrupting noise that affects the fidelity of the signal in the image (expressed in decibels).

Table 5. Quantitative Analysis for Evaluation Parameters

Sl. No	Gray value	FSIM	SSIM	Contrast	Time Period	MSE	PSNR
1	0.62	0.87	0.97	62.4	8.3	21.2	21.1
2	0.67	0.86	0.96	66.3	8.9	14.8	14.9
3	0.82	0.84	0.98	67.5	7.5	15.6	15.5
4	0.75	0.89	0.98	68.8	7.6	18.7	18.6
5	0.86	0.86	0.97	66.8	9.8	26.8	26.7
6	0.92	0.84	0.96	62.7	8.9	24.5	24.6
7	0.87	0.85	**0.99**	66.1	6.9	21.5	21.4
8	0.86	0.82	0.98	68.9	7.2	21.8	21.7
9	0.81	0.86	0.97	62.3	9.5	26.4	26.3
10	0.76	0.84	0.99	68.9	8.6	18.6	18.5
11	0.68	0.85	0.97	69.7	7.6	19.4	19.5
12	**0.97**	0.87	0.97	68.9	8.2	17.6	17.7
13	0.82	0.82	0.98	62.3	8.0	18.0	18.1
14	0.93	0.86	0.96	68.9	9.4	18.3	18.4
15	0.83	0.82	0.95	68.7	8.6	20.5	20.6
16	0.84	0.81	0.98	62.3	9.4	21.3	21.2
17	0.86	0.83	0.97	64.8	8.6	20.7	20.6
18	0.64	0.84	0.96	62.8	6.9	20.9	20.8
19	0.67	0.82	0.98	64.5	7.2	23.8	23.9
20	0.84	0.80	0.97	69.4	7.6	24.5	24.6
21	0.85	0.84	0.97	65.5	8.1	20.1	20.2
22	0.96	**0.89**	0.98	68.5	7.6	18.6	18.7
23	0.87	0.86	0.97	**69.7**	8.2	19.5	19.6
24	0.74	0.88	0.95	68.2	8.4	16.3	16.2
25	0.86	0.86	0.98	61.5	8.6	18.6	18.7
26	0.81	0.88	0.97	65.3	8.9	17.5	17.5
27	0.73	0.87	0.99	68.4	6.5	19.4	19.3
28	0.81	0.86	0.96	68.0	8.1	20.5	20.6
29	0.75	0.82	0.98	68.5	7.8	24.6	24.7
30	0.82	0.81	0.97	62.8	8.6	21.3	21.2
31	0.91	0.83	0.96	64.9	7.9	22.7	22.8
32	0.94	0.84	0.96	63.7	8.5	26.0	25.9
33	0.90	0.86	0.97	61.3	9.5	25.7	25.6
34	0.94	0.87	0.96	68.5	9.4	28.9	29.0
35	0.86	0.82	0.98	62.8	9.0	27.5	27.4
36	0.77	0.88	0.96	65.8	**6.5**	20.4	20.5
37	0.83	0.80	0.98	68.1	8.4	14.6	14.5
38	0.69	0.81	0.97	67.8	6.4	17.8	17.9
39	0.72	0.85	0.97	66.5	8.6	21.5	21.4
40	0.82	0.86	0.96	65.3	9.4	23.5	23.6
41	0.91	0.87	0.99	61.8	6.7	19.8	19.9
42	0.80	0.79	0.97	62.4	6.4	16.5	16.4

Mean	**0.82**	**0.84**	**0.97**	**65.91**	**8.15**	**20.8**	**20.8**

3.2.8.   *F1 score.*

The F1 score is used to evaluate the performance of the algorithm. It is obtained by

$$F1\ Score = \frac{2*(P*R)}{P+R} \qquad (3)$$

Where, P = Precision and R = Recall. From the software we obtained, P = 0.9745 and R = 0.8036. The F1 score for our proposed algorithm is 88.09%.

3.3.   *Comparison with existing work.*

The four different data sets used for evaluations are D-HAZE, SOTS, O-HAZE, and RESIDE data sets. The qualitative analysis comparison is shown in Table 6. Here we have taken 10 reference data for comparison. The quantitative analysis of different data sets with different references is shown in Table 7 and Table 8. Table 7 compares the Evaluation Parameters of SSIM and FSIM. Table 8 differentiates the time period between the proposed and existing work.

Table 6. Comparison of proposed and existing work.

Sl. no	Input	Output					
		Proposed results	Ju, Mingye et al. 2021	Rinky, B.P et al. 2012	Ma, Shaojin et al. 2023	Zhang et al. 2021	Liu et al. 2021
1							
2							
3							
4							
5							
6							
7							
8							
9							
10							

Table 7. Quantitative comparison of FSIM and SSIM

Sl. no	References	O-HAZY		SOTS		D-HAZY		RESIDE	
		FSIM	SSIM	FSIM	SSIM	FSIM	SSIM	FSIM	SSIM
1	Berman et al.	0.79	0.93	0.73	0.92	0.80	0.94	0.79	0.95
2	Gu, Zhenfei et al.	0.78	0.94	0.79	**0.96**	0.76	0.95	0.8	0.96
3	Ju, Mingye et al.	0.73	0.93	0.81	0.94	**0.83**	0.96	0.76	0.96
4	Jiang, Bo et al.	0.8	0.92	0.78	0.92	0.72	0.93	0.79	0.94
5	Lin et al.	0.83	0.89	**0.87**	0.95	0.76	0.96	0.72	**0.97**
6	Liu, Juping et al.	0.76	0.94	0.76	0.92	0.71	0.93	0.79	0.95
7	Mohideen et al.	0.83	0.96	0.78	0.93	0.79	**0.97**	0.78	0.95
8	Rinky, B.P et al.	0.79	**0.98**	0.81	0.95	0.75	0.96	**0.85**	0.92
9	Xu, Hao et al.	0.81	0.95	0.79	0.94	0.73	0.95	0.73	0.95
10	Zhuang et al.	**0.86**	0.96	0.75	0.94	0.79	0.95	0.76	0.95
	Proposed Work	**0.845**	**0.971**	**0.856**	**0.973**	**0.832**	**0.969**	**0.812**	**0.968**

Table 8. Quantitative analysis of Time period.

Reference	Berman et al.	Hsu et al.	IEEE	Jiang, Bo et al.	Liu, Juping et al.	Norouzi, Alireza et al.	Tripathi et al.	Zhuang et al.	Proposed work
SOTS dataset	9.5	9.5	**8.6**	9.8	9.5	8.7	9.8	9.5	**8.3**
O-Haze dataset	8.9	**8.6**	9.8	8.9	9.9	8.6	9.8	**8.6**	**8.4**
RESIDE dataset	8.7	8.6	9.7	9.8	9.4	8.5	**8.4**	9.4	**8.1**

3.4.   Discussion.

   Table 6 shows that our SSIM and FSIM results are better than the other's work. Since some of the values are better than our results, they can be obtained only in specific datasets. For example, reference [9] is getting a good result in SSIM for O-haze and FSIM for the RESIDE dataset, but the overall (average) result will be lesser than our results. Table 7 gives the time period for our proposed work, which is lower than the other works. By these results, we can propose that our work is flawless. With the help of comparing the image quality parameters with existing papers, our proposed method for image dehazing can be claimed to be better than others.

4.   Conclusion

   We describe an efficient method for reducing image hazes. An examination of the built-in boundary constraint of the transmission function is extremely valuable to our method. An efficient variable splitting algorithm can solve the optimization problem. When compared to prior work, our approach can yield very visually

pleasing outcomes with correct color and crisper image elements and structures. There is often conflict between image color and texture during dehazing. In terms, of the effects of hazes in an unpolluted pixel might have an identical hue to the effects of fog in a polluted pixel. For example, the hazes frequently confuse the color of various white objects in the scene. It was also reduced here by using transmission tuning methods. When paired with the best techniques, the border constraint proves to be remarkably effective for dehazing most natural images, even though it places a much weaker restriction on the dehazing process. This may assist in avoiding multiple improper image enhancements and removing the uncertainty between color and depth.

CONFLICTS OF INTEREST

Regarding the publishing of this paper, the authors state that they have no conflicts of interest.

ACKNOWLEDGEMENTS

References

[1]   N. S. Pal, S. Lal, and K. Shinghal, "Modified Visibility Restoration-Based Contrast Enhancement Algorithm for Colour Foggy Images," *IETE Tech. Rev.*, vol. 35, no. 3, pp. 223–236, 2018, doi: 10.1080/02564602.2016.1276868.

[2]   Z. Lin and H. Wang, "Efficient image encryption using a chaos-based PWL memristor," *IETE Tech. Rev. (Institution Electron. Telecommun. Eng. India)*, vol. 27, no. 4, pp. 318–325, 2010, doi: 10.4103/0256-4602.64605.

[3]   W. Y. Hsu and Y. S. Chen, "Single Image Dehazing Using Wavelet-Based Haze-Lines and Denoising," *IEEE Access*, vol. 9, no. Ll, pp. 104547–104559, 2021, doi: 10.1109/ACCESS.2021.3099224.

[4]   A. K. Tripathi and S. Mukhopadhyay, "Removal of fog from images: A review," *IETE Tech. Rev. (Institution Electron. Telecommun. Eng. India)*, vol. 29, no. 2, pp. 148–156, 2012, doi: 10.4103/0256-4602.95386.

[5]   B. P. Rinky, P. Mondal, K. Manikantan, and S. Ramachandran, "DWT based Feature Extraction using Edge Tracked Scale Normalization for Enhanced Face Recognition," *Procedia Technol.*, vol. 6, pp. 344–353, 2012, doi: 10.1016/j.protcy.2012.10.041.

[6]   A. Rad, M. S. Mohd Rahim, A. Rehman, A. Altameem, and T. Saba, "Evaluation of current dental radiographs segmentation approaches in computer-aided applications," *IETE Tech. Rev. (Institution Electron. Telecommun. Eng. India)*, vol. 30, no. 3, pp. 210–222, 2013, doi: 10.4103/0256-4602.113498.

[7]   A. Norouzi *et al.*, "Medical image segmentation methods, algorithms, and applications," *IETE Tech. Rev. (Institution Electron. Telecommun. Eng. India)*, vol. 31, no. 3, pp. 199–213, 2014, doi: 10.1080/02564602.2014.906861.

[8]   S. K. Mohideen, S. A. Perumal, and M. M. Sathik, "Image De-noising using Discrete Wavelet transform," *Int. J. Comput. Sci. Netw. Secur.*, vol. 8, no. 1, pp. 8–11, 2008.

[9]   Institute of Electrical and Electronics Engineers. Kerala Section, IEEE Region 10, and Institute of Electrical and Electronics Engineers, *Proceedings of the TENCON 2019 : Technology, Knowledge, and Society : 17-20 October 2019, Grand Hyatt Kochi Bolgatti, Kerala, India.*

[10]   Z. Gu, M. Ju, and D. Zhang, "A Single Image Dehazing Method Using Average Saturation Prior," *Math. Probl. Eng.*, vol. 2017, 2017, doi: 10.1155/2017/6851301.

[11]   S. B. Borkar and S. V Bonde, "Oceanic Image Dehazing based on Red Color Priority using Segmentation Approach," 2017. [Online]. Available: http://www.ripublication.com

[12]   B. Jiang *et al.*, "A Dehazing Method for Remote Sensing Image under Non-uniform Hazy Weather Based on Deep Learning Network," *IEEE Trans. Geosci. Remote Sens.*, 2023, doi: 10.1109/TGRS.2023.3261545.

[13]   D. Berman, T. Treibitz, and S. Avidan, "Single Image Dehazing Using Haze-Lines," *IEEE Trans. Pattern Anal. Mach. Intell.*, vol. 42, no. 3, pp. 720–734, Mar. 2020, doi: 10.1109/TPAMI.2018.2882478.

[14]   M. Ju, C. DIng, C. A. Guo, W. Ren, and D. Tao, "IDRLP: Image Dehazing Using Region Line Prior," *IEEE Trans. Image Process.*, vol. 30, pp. 9043–9057, 2021, doi: 10.1109/TIP.2021.3122088.

[15]   S. Ma *et al.*, "Image Dehazing Based on Improved Color Channel Transfer and Multiexposure Fusion," *Adv. Multimed.*, vol. 2023, pp. 1–10, May 2023, doi: 10.1155/2023/8891239.

[16]   L. Zhuang, Y. Ma, Y. Zou, and G. Wang, "A Novel Image Dehazing Algorithm via Adaptive Gamma-

Correction and Modified AMEF," *IEEE Access*, vol. 8, pp. 207275–207286, 2020, doi: 10.1109/ACCESS.2020.3038239.

[17]   R. Sethi and S. Indu, "Local Enhancement of SLIC Segmented Underwater Images using Gray World based Algorithm," *2017 9th Int. Conf. Adv. Pattern Recognition, ICAPR 2017*, pp. 3–8, 2018, doi: 10.1109/ICAPR.2017.8593151.

[18]   Z. Huang, H. Jing, A. Chen, C. Hong, and X. Shang, "Efficient image dehazing algorithm using multiple priors constraints," *J. Vis. Commun. Image Represent.*, vol. 90, Feb. 2023, doi: 10.1016/j.jvcir.2022.103694.

[19]   J. Zhang, F. Feng, and W. Song, "A compensation textures dehazing method for water alike area," *J. Supercomput.*, vol. 77, no. 4, pp. 3555–3570, Apr. 2021, doi: 10.1007/s11227-020-03406-8.

[20]   H. Xu, Y. Tan, W. Wang, and G. Wang, "Image Dehazing by Incorporating Markov Random Field with Dark Channel Prior," *J. Ocean Univ. China*, vol. 19, no. 3, pp. 551–560, Jun. 2020, doi: 10.1007/s11802-020-4003-6.

[21]   J. Liu, S. Wang, X. Wang, M. Ju, and D. Zhang, "A review of remote sensing image dehazing," *Sensors*, vol. 21, no. 11. MDPI AG, Jun. 01, 2021. doi: 10.3390/s21113926.

[22]   Y. Hole, S. Hole, L. P. Leonardo Cavaliere, B. Nair, M. Hasyim and H. B. Bapat, (2023) "Blockchain Usages in Hospitality Management," 2023 3rd International Conference on Advance Computing and Innovative Technologies in Engineering (ICACITE), Greater Noida, India, 2023, pp. 2798-2801, doi: 10.1109/ICACITE57410.2023.10183291.

[23]   Y. Hole, S. Hole, A. A. Ayub Ahmed, E. Efendi, I. Ibrahim and M. Hasyim, (2023) "Internet of Things Issues and Challenges," 2023 3rd International Conference on Advance Computing and Innovative Technologies in Engineering (ICACITE), Greater Noida, India, 2023, pp. 1370-1373, doi: 10.1109/ICACITE57410.2023.10183221.